

Numerical Investigation of Buoyancy-driven Flow in a Crescent-shaped Enclosure

Housseem Laidoudi¹, Ahmed Kadhim Hussein^{2,3}, Ahmed B. Mahdi⁴, Obai Younis^{5,6,*},
Emad Hasani Malekshah⁷, Hussein Togun⁸, Uddhaba Biswal⁹

¹Laboratory of Sciences and Marine Engineering, Faculty of Mechanical Engineering, USTO-MB, BP 1505, El-Menaouer, Oran, 31000, Algeria.

²College of Engineering - Mechanical Engineering Department – University of Babylon - Babylon City – Hilla – Iraq.

³College of Engineering, University of Warith Al-Anbiyaa, Karbala, Iraq

⁴Anesthesia Techniques Department, Al-Mustaqbal University College, Babylon, Iraq.

⁵Department of Mechanical Engineering, College of Engineering at Wadi Addwaser, Prince Sattam Bin Abdulaziz University, Wadi Addwaser, KSA

⁶Department of Mechanical Engineering, Faculty of Engineering, University of Khartoum, Khartoum, Sudan ⁷Department of Power Engineering and Turbomachinery, Silesian University of Technology, Gliwice 44-100, Poland

⁸Department of Biomedical Engineering, University of Thi-Qar, Iraq

⁹Department of Mathematics, National Institute of Technology Rourkela, Rourkela 769008, Odisha, India

Received 22 Jun 2022

Accepted 18 Jul 2022

Abstract

The buoyancy-driven flow in a crescent cavity is numerically analyzed by employing the finite volume method for the first time. The enclosure was filled with an incompressible fluid, whose thermal properties are given by Pr. The enclosure's left and right arcs have different temperatures. Two cases are adopted in the present work; in the first case, the left and right arcs were considered cold and hot. While for the second case, the thermal boundary conditions of the arcs were shifted. The results were illustrated for Prandtl number $0.71 \leq Pr \leq 50$ blockage ratio of the space $0.1 \leq B \leq 0.5$ and Rayleigh number $103 \leq Ra \leq 105$. For both considered cases, the velocity profiles increased with the increasing Ra and decreasing B. While the increase in Ra increases the values of Nu for both arcs. Also, the flow and thermal pattern are not affected by changing the fluid's thermal properties represented by Pr. Furthermore, when the influence of buoyant force is substantial, and the cavity width is wide, the shifting thermal boundary conditions become evident. These new results can be exploited in heat exchanger applications as well as insulating systems.

© 2022 Jordan Journal of Mechanical and Industrial Engineering. All rights reserved

Keywords: Natural convection, Crescent-shaped cavity, FVM.

Nomenclature

Symbol	Description	Unit	
B	The blockage ratio of the space		X Non-dimensional coordinate in the horizontal direction
g	Gravitational acceleration	m/s ²	y Coordinate in the vertical direction m
d	Width of the gap inside the cavity	m	Y Non-dimensional coordinate in the vertical direction
H	Cavity height	m	
n	Normal vector		
Nu	Mean Nusselt number		
p	Pressure	N/m ²	
P	Nondimensional pressure		
Pr	Prandtl number		
Ra	Rayleigh number		
T	Temperature	°C	
u	Velocity component in x-direction	m/s	
U	Non-dimensional velocity component in X-direction		
v	Velocity component in y-direction	m/s	
V	Non-dimensional velocity component in Y-direction		
x	Coordinate in the horizontal direction	m	

Greek Symbols

α	Thermal diffusivity	m ² /s
β	Thermal expansion coefficient	K ⁻¹
ϕ	Non-dimensional temperature	
ν	Kinematic viscosity	m ² /s
ρ	Density	kg/m ³

Subscripts

c	Cold
h	Hot
l	Local

* Corresponding author e-mail: oubeytaha@hotmail.com.

1. Introduction

The buoyancy-driven convection, or sometimes called the free convection, in enclosures is a topic of great interest in heat transfer. This famous problem has received wide interest in the scientific community [1-3]. This is not a sudden chance, but it is due to its huge practical applications. These applications include nuclear reactors, thermal storage systems, cooling of electronic equipment, solar energy, heat exchangers, refrigerators, melting and solidification, drying and food technologies, wet clutches and airplane cabin insulation [4-9]. Unfortunately, most of the published papers on this problem are concerned with the classical well-known square or rectangular geometries. Whereas the papers concerned with the complicated geometries are much less than that related to the classical geometries. Samples of the complicated cavities include triangular [10-13], vee-corrugated [14-16], wavy [17], elliptical [18], parallelogrammic [19-22], trapezoidal [23], parabolic [24], C-shape [25], T-shape [26], L-shape [27], Γ -shape [28], U-shape [29] and F-shape [30].

Dutta et al. [31] examined entropy production and natural convection inside a rhombic enclosure with a wavy and non-uniformly heated upper wall by numerical means. Whereas its lower and sidewalls were kept cold. They deduced that the Nu_{av} was enhanced with the increase in the tilting angle. Hussein [32] explored the influence of the hot concentric circular cylinder on the free convection inside a parallelogrammic cavity loaded with air. He concluded that the increase in Ra enhanced the Nu_{av} values. The numerical investigation of the free convective flow inside a parallelogrammic enclosure with cold sidewalls was investigated by Salih and Mustafa [33]. The lower wall was partially heated, whereas the rest of this wall, together with the upper wall, were isolated. The authors deduced that Nu_{av} was enhanced by increasing the heat source length for all values of Ra and the cavity's inclination angle. The impact of various boundary conditions on free convection inside a porous parallelogrammic cavity was numerically addressed by Anandalakshmi and Basak [34]. The results revealed that the Nu_{av} was enhanced for high Da for Rayleigh-Benard boundary condition. The numerical investigation of MHD buoyancy-driven convective flow inside an enclosure cavity elliptic shape was made by Adekeye et al. [35]. The cavity was loaded with a fluid saturated with a porous media, a hot top wall and a cold bottom wall. The authors reported that the impact of the tilted angle on the heat transmission rate was significant at $58^\circ \leq \phi \leq 90^\circ$. The numerical analysis of the free convection inside an octagonal enclosure included, inside it, a hot solid circular cylinder was presented by Hussain and Hussein [36]. All enclosure walls were cold. The cylinder was moved in three different directions (i.e., vertical, horizontal and diagonal). The study findings were presented for various Ra numbers and cylinder locations. It was found that the Nu_{av} attained its peak value at the highest Ra . Chen and Cheng [37] numerically and experimentally analyzed the buoyancy-driven convection of air in a tilted arc-shaped cavity. It was found that the increase in Gr intensified the Nu_{av} . Also, they observed that the vortex pattern was affected by the values of inclination angles. The numerical examination of the buoyancy-driven convective flow inside an inclined cavity of L-shape loaded with Newtonian fluid was performed by Tasnim and Mahmud [38]. They deduced that there was a linear relationship

between (Nu_{av} and the tilted angle of the cavity at $AR = 0.25$ and $Ra = 10^3$ and 10^4). Mustafa [39] explored air free convective flow confined in a parabolic enclosure with cold vertical walls numerically. The upper wall of the cavity was thermally isolated, while the lower one was hot. It was found that the highest Ra and small value of the parabolic equation maximized the Nu_{av} values. Wang et al. [40] numerically explored air convective flow inside a circular cavity containing a hot flat plate. The outer cavity wall was maintained at an isothermal cold temperature. The results indicated that the Nu_{av} was intensified when the flat plate was located vertically inside the cavity. Wang et al. [41] researched the impact of the orientation of the internal cylinder on the natural convective flow inside a cavity of a circular geometry numerically. The authors deduced that the local Nusselt number was enhanced when the cylinder was located in the corner-upward orientation. The numerical study of natural convection in a 3D spherical enclosure with cold external walls was performed by Welhezi et al. [42]. The cavity included a hot cubical body filled with various kinds of fluids. The results indicated that the Nu_{av} was maximized at $Pr = 25$ and $Ra = 10^7$. The numerical analysis of the free convective flow inside an isosceles triangular cavity was conducted by Roy et al. [43]. The enclosure's bottom wall was heated in a uniform and non-uniform manner. The local Nusselt number was shown to have an oscillating tendency. Saha [44] numerically analyzed transient laminar free convective flow inside a triangular cavity having hot inclined walls. The bottom wall of it was kept thermally insulated. He deduced that the instantaneous Nu_{av} strongly depended on Pr , Ra and the cavity aspect ratio. Oztop et al. [45] considered natural convection inside a tilted triangular cavity heated from below. The vertical wall was hot, while the inclined one was cold. The authors deduced that the heat transmission was influenced by the inclination angle and Ra . El-Hassan et al. [46] numerically researched natural convection inside a gamma of right-angled triangular enclosures. The upper walls were kept thermally insulated, whereas the inclined wall was cold and the vertical one was hot. They deduced that the Nu_{av} was related to the cavity cross-sectional area. Yesiloz and Aydin [47] conducted a computational and experimental study on free convection inside a triangular enclosure loaded with water. The vertical, bottom, and inclined walls were cold, hot and thermally insulated, respectively. They recommended a correlation of Nu as a function of the Ra . The buoyancy-driven convective flow inside a tilted enclosure bounded by adiabatic horizontal flat walls was examined by Mushatet [48]. The enclosure's sidewalls were wavy and preserved at hot temperatures. He deduced that the local Nusselt number was reduced with higher values of wavy wall amplitude. Adjlout et al. [49] numerically analyzed free convection inside an inclined chamber with an insulated horizontal wall. The flat left and wavy right sidewalls were considered cold and hot, respectively. The results indicated that the increase in the number of undulations decreased the heat transmission rate when the tilt angle was more than 75° . Koulali et al. [50] numerically examined natural convective flow inside a corrugated enclosure with two superimposed fluid layers. The upper and lower walls were kept adiabatic and under a constant heat flux, respectively, whereas the vertical walls were assumed cold. They found that the corrugated wall improved the heat transmission in the cavity. The numerical examination of the buoyancy-driven convective flow inside a tilted trapezoidal enclosure was performed by

Hussein et al. [51]. Both its sidewalls were assumed cold, whereas the lower and upper walls were hot and adiabatic, respectively. They concluded that the Nu_{av} attained its peak value at a tilt angle equal to (30°). Natarajan et al. [52] numerically explored the free convection inside a trapezoidal enclosure with cold sidewalls and a top adiabatic wall. The enclosure's bottom wall was heated either uniformly or non-uniformly. They concluded that the Nu_{av} was decreased for the non-uniform heating case. The numerical analysis of the buoyancy-driven convection inside an inclined trapezoidal enclosure was introduced by Lasfer et al. [53]. Both upper and lower walls were assumed adiabatic. Whereas the inclined left sidewall was hot, and the vertical right sidewall was cold. It was deduced that the Nu_{av} was a function of the aspect ratio, Ra and the inclination angle. Additional works related to the buoyancy-driven convection in complex shape cavities can be found in [54-63]. Based on the comprehensive literature and our wide experience in the convection heat transfer, there has been no research to date that has quantitatively explored free convection inside a crescent shape cavity. So, the contribution of the current work is to research this novel problem in more detail and with intense attention.

2. The physical model, governing equations and boundary conditions

Fig. 1 shows the physical model for a crescent-shaped cavity formed by meeting its inner and outer arcs. Also, the cavity height is defined by H , and the width of the gap inside the cavity is defined by d . The ratio d/H is called the blockage ratio B , and it is selected between (0.1 and 0.5). The cavity's left and right arcs have different temperatures. Two cases are adopted in the present work; in the first case, the left and right arcs were considered cold and hot. Whereas, in the second case, the left and right arcs were considered hot and cold, respectively. The cavity was filled with an incompressible fluid, whose thermal properties are given by Pr . The temperature difference between these arcs is responsible for making the thermal buoyancy force driving the natural convection inside the cavity.

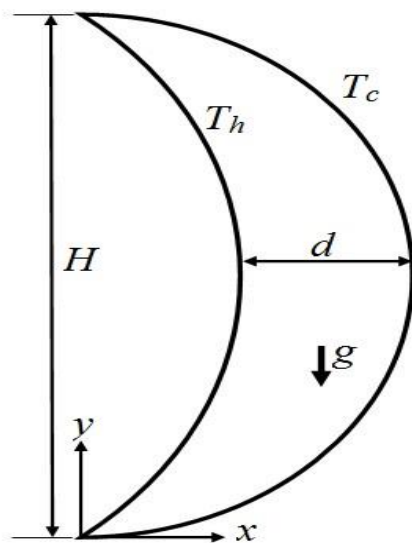


Figure1. Physical representation of the crescent cavity.

Before describing the mathematical model, it is worth presenting the assumptions are used in this work:-

1. No-slip condition is assumed between the fluid and the solid arcs of the cavity.
2. The flow is 2 D, steady, laminar and Newtonian.
3. The thermo-physical characteristics of the fluid are not related to temperature except the density, which was dealt with by the Boussinesq approximation.
4. In this type of work, the physical phenomena are not related to time, so the equations for this work are not related to time.

The dimensionless form of the governing continuity, momentum and energy equations in the Cartesian coordinate system read [3-6]:

$$\frac{\partial U}{\partial X} + \frac{\partial V}{\partial Y} = 0 \quad (1)$$

$$\frac{\partial U}{\partial X} U + \frac{\partial U}{\partial Y} V = -\frac{\partial P}{\partial X} + Pr \left(\frac{\partial^2 U}{\partial X^2} + \frac{\partial^2 U}{\partial Y^2} \right) \quad (2)$$

$$\frac{\partial V}{\partial X} U + \frac{\partial V}{\partial Y} V = -\frac{\partial P}{\partial Y} + Pr \left(\frac{\partial^2 V}{\partial X^2} + \frac{\partial^2 V}{\partial Y^2} \right) + Ra \cdot Pr \cdot \phi \quad (3)$$

$$\frac{\partial \phi}{\partial X} U + \frac{\partial \phi}{\partial Y} V = \left(\frac{\partial^2 \phi}{\partial X^2} + \frac{\partial^2 \phi}{\partial Y^2} \right) \quad (4)$$

The last term in Eq.(3) illustrates Y-direction's connection between the momentum and energy equations. Eqs. (1-4) are presented in nondimensional form after converting the dimensional parameters in this way:

$$X = \frac{x}{H}, Y = \frac{y}{H}, U = \frac{uH}{\alpha}, V = \frac{vH}{\alpha}, P = \frac{pH^2}{\rho\alpha^2}, \phi = \frac{T-T_c}{T_h-T_c} \quad (5)$$

While the Prandtl and Rayleigh numbers in the above equations are expressed as follows

[64] :

$$Pr = \frac{\nu}{\alpha}, Ra = \frac{g\beta(T_h - T_c)H^3}{\nu\alpha} \quad (6)$$

$Pr = 0.71, 6.1$ and 50.071 for air, 6.1 for water and 50 for oil.

The Prandtl number expresses the thermal properties of the fluid. Whereas the Rayleigh number indicates the intensity of the thermal buoyancy inside the cavity. Convection heat transmission is evident in the cavity due to the temperature difference between the fluid and the enclosure's arcs. The values of the heat transfer rate are expressed by the local and mean Nusselt numbers as follows:

$$Nu_t = \left. \frac{\partial \phi}{\partial n} \right|_{wall} \quad (7)$$

$$Nu = \frac{1}{s} \int_0^s Nu_t ds \quad (8)$$

The Nu represents the mean of local values of the Nusselt number. That means the value of Nu increases with increasing the temperature gradient.

To complete the mathematical model, the appropriate boundary conditions must be specified as follows [3-6]:

For the cold arc of the cavity

$$U = 0, V = 0, \phi = 0 \quad (9)$$

For the hot arc of the cavity

$$U = 0, V = 0, \phi = 1 \quad (10)$$

3. Simulation procedure and the numerical test

To achieve the numerical simulation of the current study, a set of points must be accomplished and verified. These points can be summarized into two main parts as follows:

- Creating the grids and checking the density of their elements to minimize the error in the numerical results.
- Verifying the used numerical model.

The code Gambit is used to draw and create the grids of the studied space. Fig. 2 depicts the shape of the grid after its completion. The density of the elements was verified in each case from the value of the ratio (B). The results of this verification are shown in Table 1. It can be concluded that the element numbers for (case 2) are sufficient to reach satisfactory results. So, this step is called grid independency test.

The numerical code (ANSYS-CFX) was used as a solver in this investigation. The code transforms the differential equations (Eqs. (1-4)) into a matrix system by integrating the initial conditions (Eqs. 9 and 10), employing the finite volume approach. The high-resolution scheme solves the convective terms of the matrix system. While the SIMPLEC algorithm coupled the pressure and velocity. The results of the calculation can be adopted when the error becomes (10^{-8}) for momentum equations and (10^{-6}) for energy equations. To validate the numerical scheme used in this study, the natural convection problem in a square cavity at $Ra = 10^3$ and 10^5 as performed by Barakos et al. [65] is resolved again by employing the same numerical approach of the current paper. Also, this code was used to solve the previous problems considered by Kuehn and Goldstein [66] and Matin and Khan [67]. The comparison presented in Figs 3 and 4 shows that very good confidence was noticed. These comparisons confirm the accuracy of the method used.

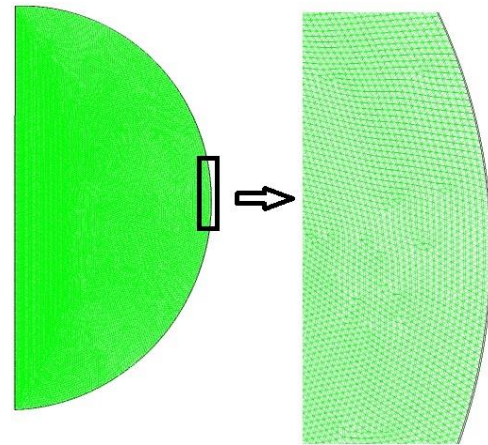


Figure 2. The shape of the created grid.

Table 1. Grid independency test for $Pr = 6.01$ and $Ra = 10^4$.

B	Case	Number of elements	Nu	difference
0.5	1	55275	4.4985	0.33%
	2	110550	4.5132	0.18%
	3	231100	4.5215	-
0.4	1	44220	4.3952	0.57%
	2	88440	4.4205	0.016%
	3	176880	4.4198	-
0.3	1	35376	4.2262	2.20%
	2	70752	4.3217	0.12%
	3	141504	4.3165	-
0.2	1	28301	4.1984	0.89%
	2	56602	4.2362	0.16%
	3	113204	4.2432	-
0.1	1	22641	4.1291	0.87%
	2	45282	4.0931	0.62%
	3	90564	4.0674	-

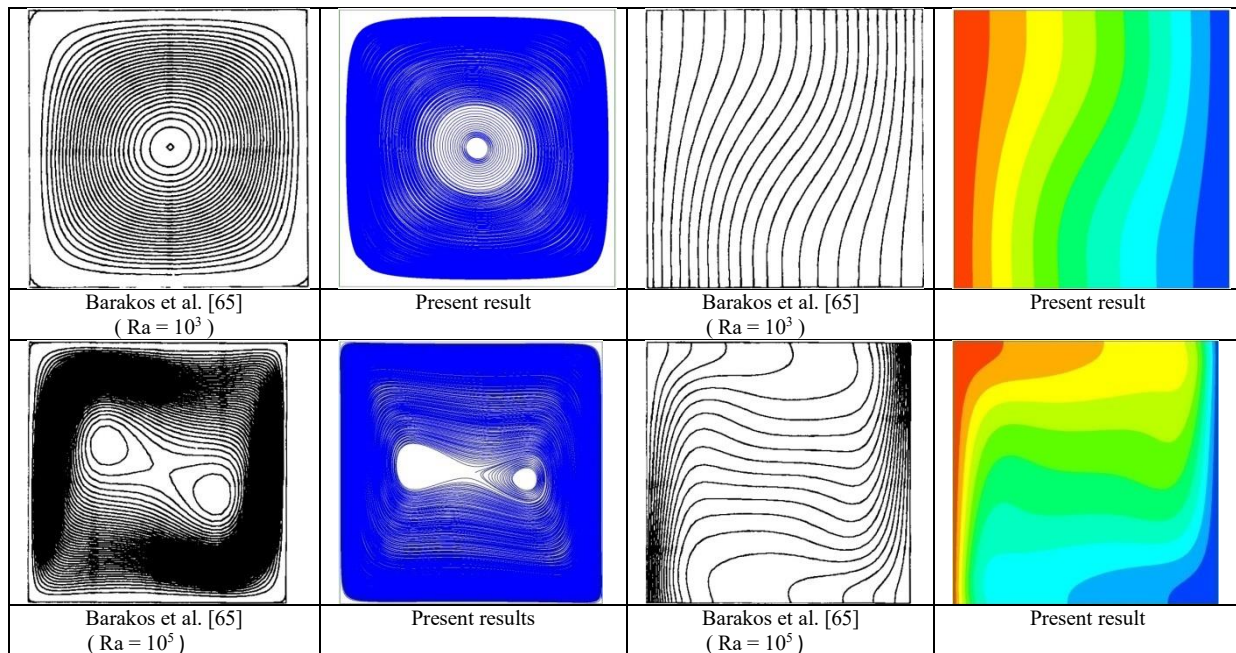


Figure 3. Comparison of streamlines (left) and isotherms (right) between current study results and Barakos et al. [65] results for $Pr = 6.1$.

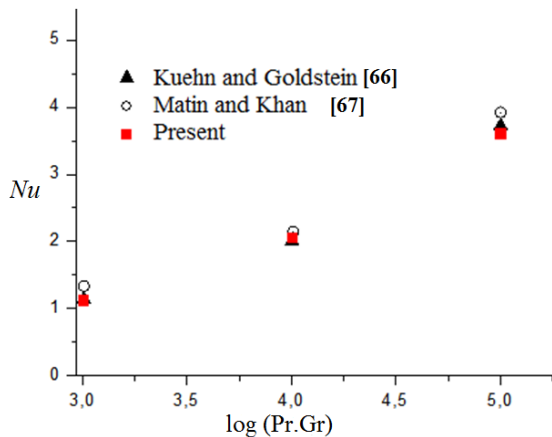


Figure 4. Comparison of Nu values of current study results and the results of Kuehn and Goldstein [66] and Matin and Khan [67] at $Pr = 6.2$.

4. Results and discussion

The buoyancy-driven flow of a fluid trapped in a room with a crescent shape cross-section was investigated numerically in the current study. The studied parameters are Prandtl number $0.71 \leq Pr \leq 50$, blockage ratio of the space $0.1 \leq B \leq 0.5$ and Rayleigh number $10^3 \leq Ra \leq 10^5$.

4.1. Case 1 (Cold left arc and hot right arc):

In this case, the left and right arcs of the cavity were preserved at constant cold and hot temperatures, respectively. Figs. 5 and 6 show the streamlines inside the crescent shape cavity for various values of Ra , Pr and B related to (case 1). Fig. 5 shows the impact of changing both the blockage ratio B and Ra numbers at a constant Pr number (i.e., $Pr = 6.01$). While, Fig. 6 presents the impact of changing Pr number and blockage ratio B at a constant Ra number (i.e., $Ra = 10^4$). It can be seen from both figures that the variation in the values of B has a clear effect on the cavity geometry. So, it switches from a semi-circle shape at the largest value of B or at $B = 0.5$ to a crescent shape at the lowest value of B or at $B = 0.1$. As the value of B decreases gradually, the left arc of the cavity becomes more concave to the internal space until it attains the crescent shape at $B = 0.1$. Therefore, the width of the gap inside the cavity decreases with decreasing the blockage ratio B .

Because of buoyancy force, the fluid layers near the hot right arc of the cavity become less dense and lighter, so they move upward to the top of the cavity. The fluid layers near the cold left arc become denser and heavy, moving downwards. Therefore, it can be observed from Figs. 5 and

6 that there is a circular flow inside the center of the cavity due to the flow movement between the hot and cold arcs of the cavity. The flow pattern in the cavity is uniform for lower values of Ra ($Ra < 10^4$). In this case, the viscous force is more predominant than buoyancy. Therefore, both the buoyancy force and the natural convection effects are weak. However, when the Ra value reaches $Ra = 10^5$, a definite disruption in the flow pattern may be observed. This is owing to the strong impacts of buoyant force and natural convection at high Ra .

Additionally, when the Ra number rises, the fluid velocity increases. Also, the flow vortices can be seen near the upper and lower edges of the cavity. Also, it can be observed from Figs. 5 and 6 that as the value of B decreases from $B = 0.5$ to 0.1 , the fluid movement becomes slow, and the flow pattern becomes approximately similar. Since the reduction in the value of B reduces the gap width inside the cavity and makes the region of the flow area inside it more restricted. Therefore, this hinders the movement of the flow. Furthermore, it can be observed from Fig. 6 that there is a small minor vortex at the bottom of the cavity and a major vortex at its center $B = 0.1$ and $Ra = 10^5$.

Concerning the effect of Pr on the streamline contours, it can be observed from Fig. 6 that there is no significant change in their pattern when the Pr increases from ($Pr = 0.71$) to $Pr = 50$. Therefore, it can be concluded that the flow pattern does not affect by changing the fluid's thermal properties represented by the Pr . Fig.7 illustrates the isotherms (dimensionless temperature) distribution of the fluid in the cavity in terms of the studied values of B and Ra number at $Pr = 6.1$. Since there is no effect of the Pr number values on the natural convection, as was observed in Fig. 6. Only one value of the Pr number was tested on the isotherms. When Ra number is low, the isotherm contours are symmetrical, close to each other, uniform and parallel to the arcs of the cavity. In this case, the heat is transmitted by conductive mode. Because of the high-temperature gradient in the cold arc's upper side and the hot arc's lower side, the isotherms' intensity increases in these regions. Therefore, the heat transmission was enhanced compared with the rest of the cavity. The clustering of isotherms at any point in the cavity arcs can be considered a good signal of a severe temperature gradient and a high heat transfer. At $Ra = 10^5$, the isotherm pattern changes significantly and elongates deeply, especially at the center of the cavity. Also, a thermal plume is evident within this space. In this case, convective heat transfer becomes significant.

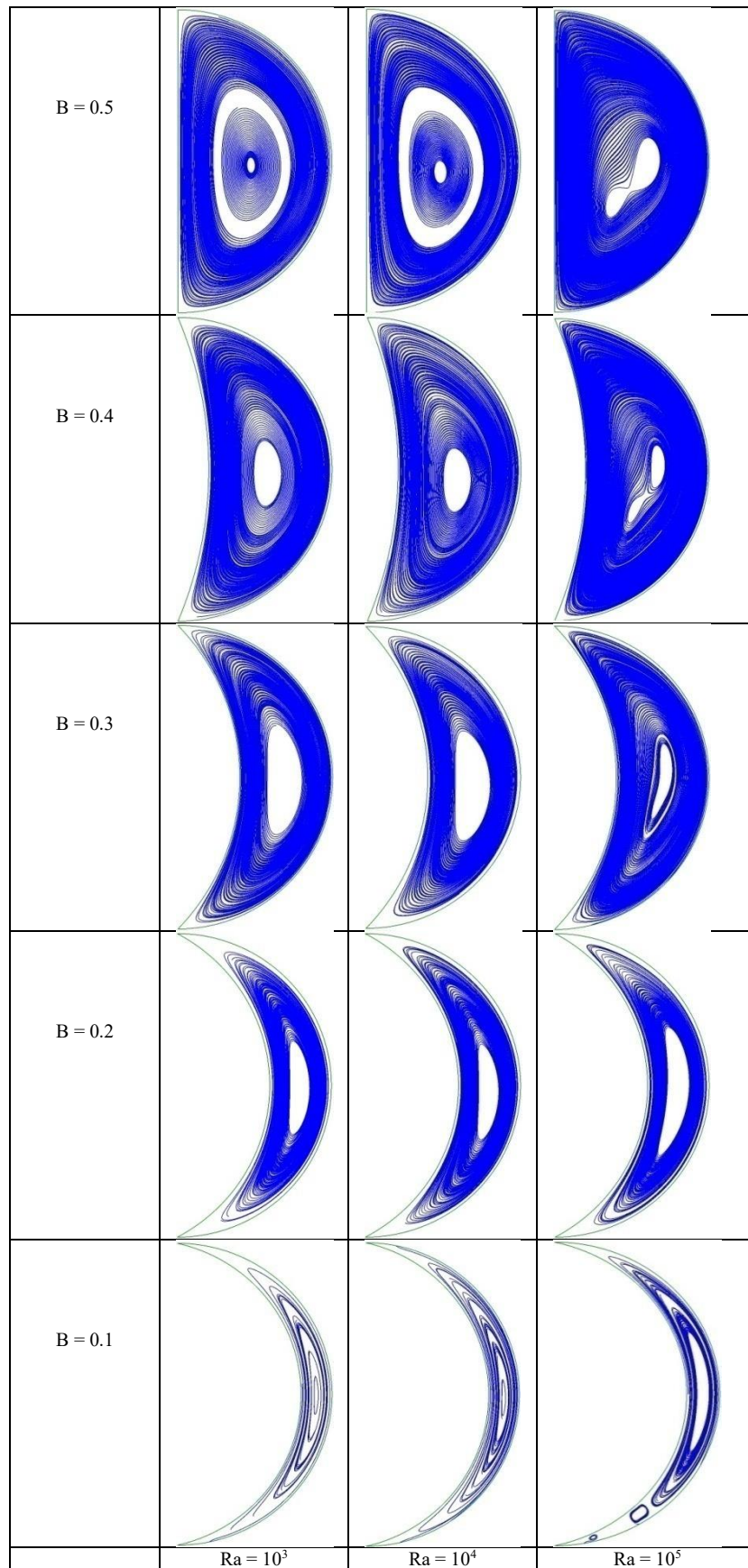


Figure 5. Streamlines inside the crescent shape cavity for various values of Ra and B at $Pr = 6.1$ related to (case 1).

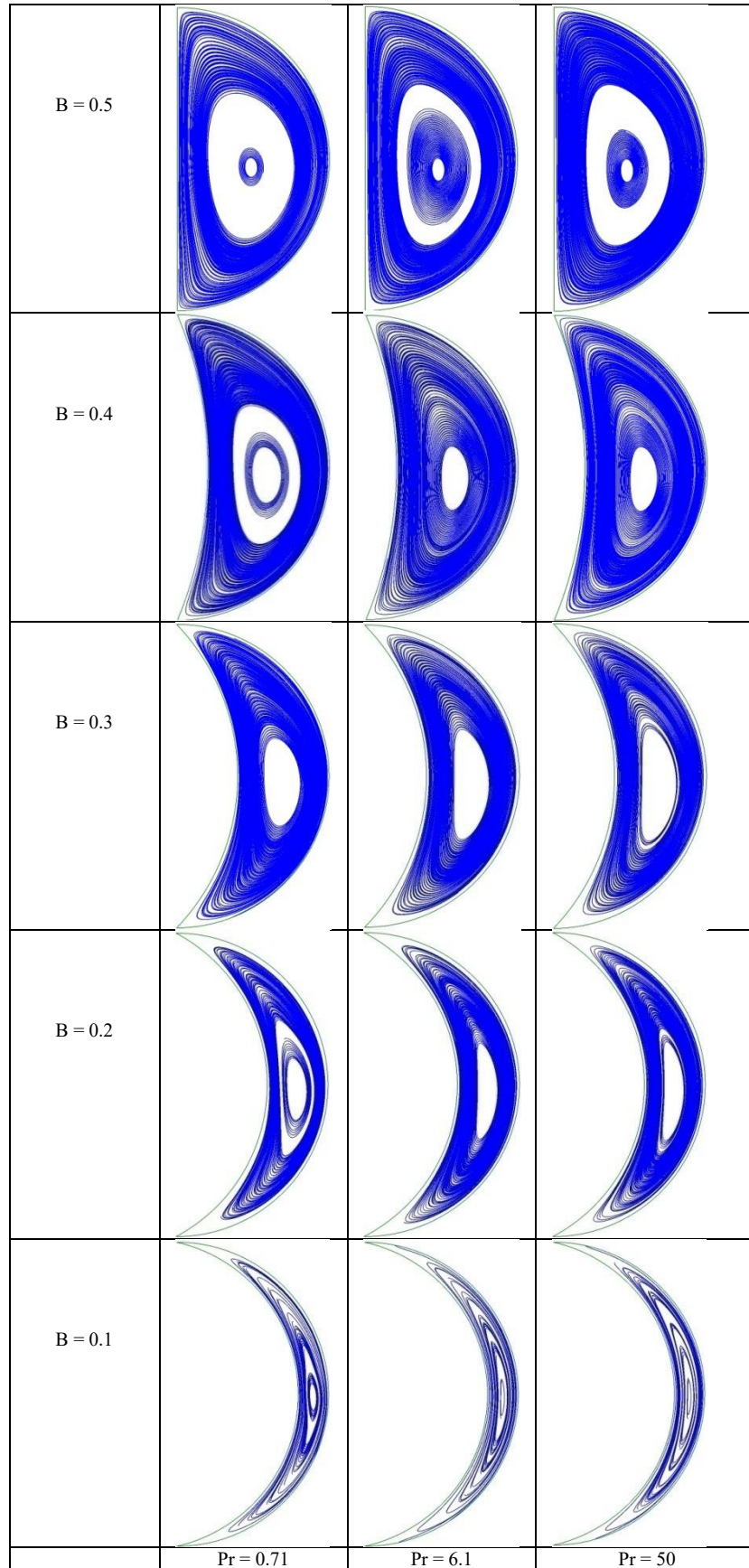


Figure 6. Streamlines inside the crescent shape cavity for various values of Pr and B at $Ra = 10^4$ related to (case 1).

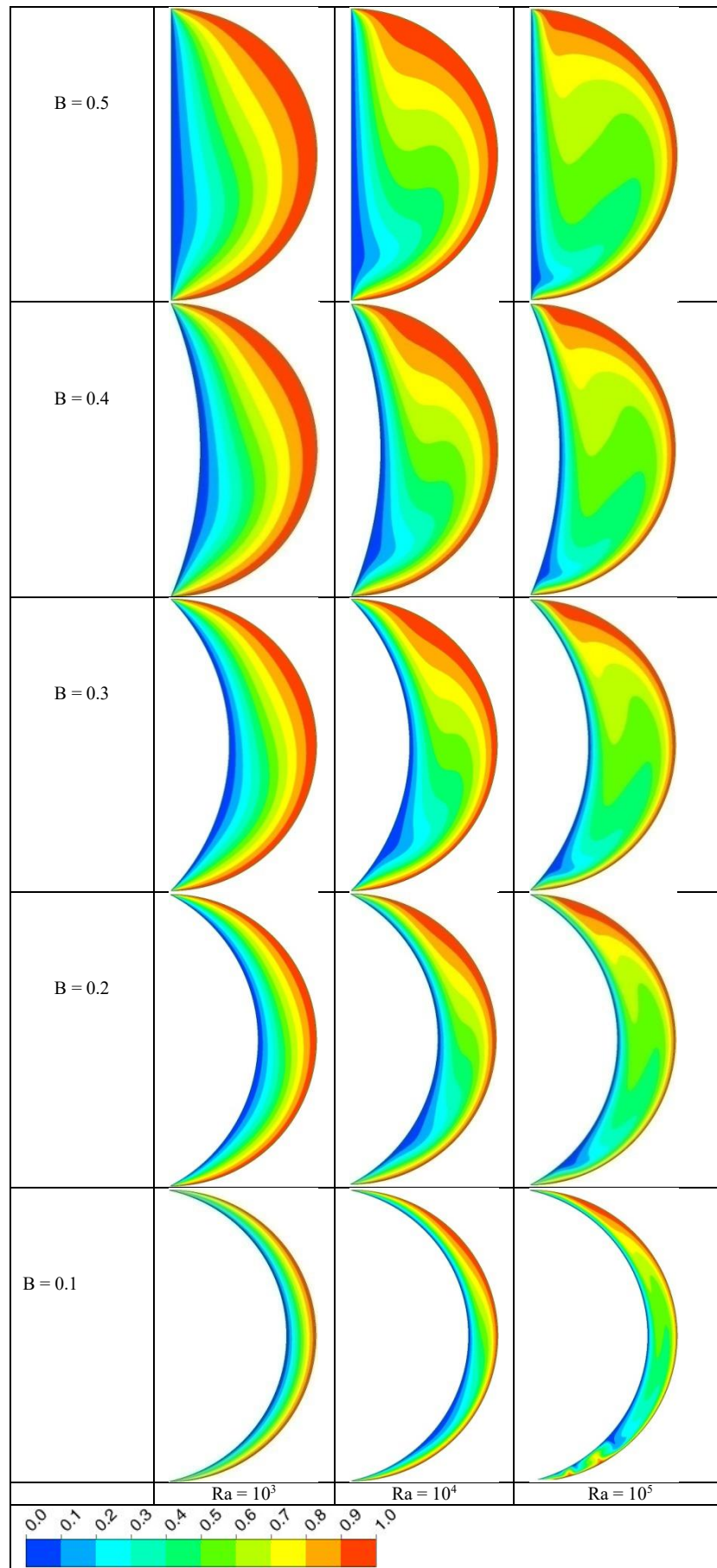


Figure 7. Isotherms inside the crescent shape cavity for various values of Ra and B at $Pr = 6.1$ related to (case 1).

Fig. 8 illustrates the distribution of dimensionless velocity component V along with the width gap spacing for various values of Ra and B at $Pr = 6.1$. The plus (+) and minus (-) signs indicate the direction of the movement of the fluid particles. This means that the flow direction is downward near the cold left arc. While near the hot right arc, its direction is upward. It could be observed that the flow velocity rises as Ra increases. In addition, at $Ra = 10^5$, the maximum velocity of the flow in the vicinity of the hot and cold arcs begins to increase by decreasing the value of B from $B = 0.5$ to 0.1 . So, the peak value corresponds to the lowest value of B .

Fig. 9 shows the profiles of the mean values of Nu in terms of Ra , Pr , and B . It can be seen that the values of Nu are affected by the variation in both Ra and B whereas there is no clear effect of the variation in Pr on their

values. It is useful to mention that the first group (the red lines) was related to the hot arc, while the second group (the blue lines) was related to the cold arc. The mean Nu values are taken in their absolute values, while the signs (+ and -) refer to the direction of the convection heat transfer. It is noticed that increasing Ra directly results in an increment in the values of Nu for both arcs. This is caused by a rise in the thermal buoyancy's magnitude, which argues the heat transfer rates for both arcs. Concerning the effect of the parameter B on the values of Nu , it is observed that as B decreases from (0.5) to (0.1), the Nu for the hot arc decreases whereas its value for the cold arc begins to increase. This means that as the cavity width decreases, the heat transmission rate of the hot arc while the heat transmission rate of the cold arc increases.

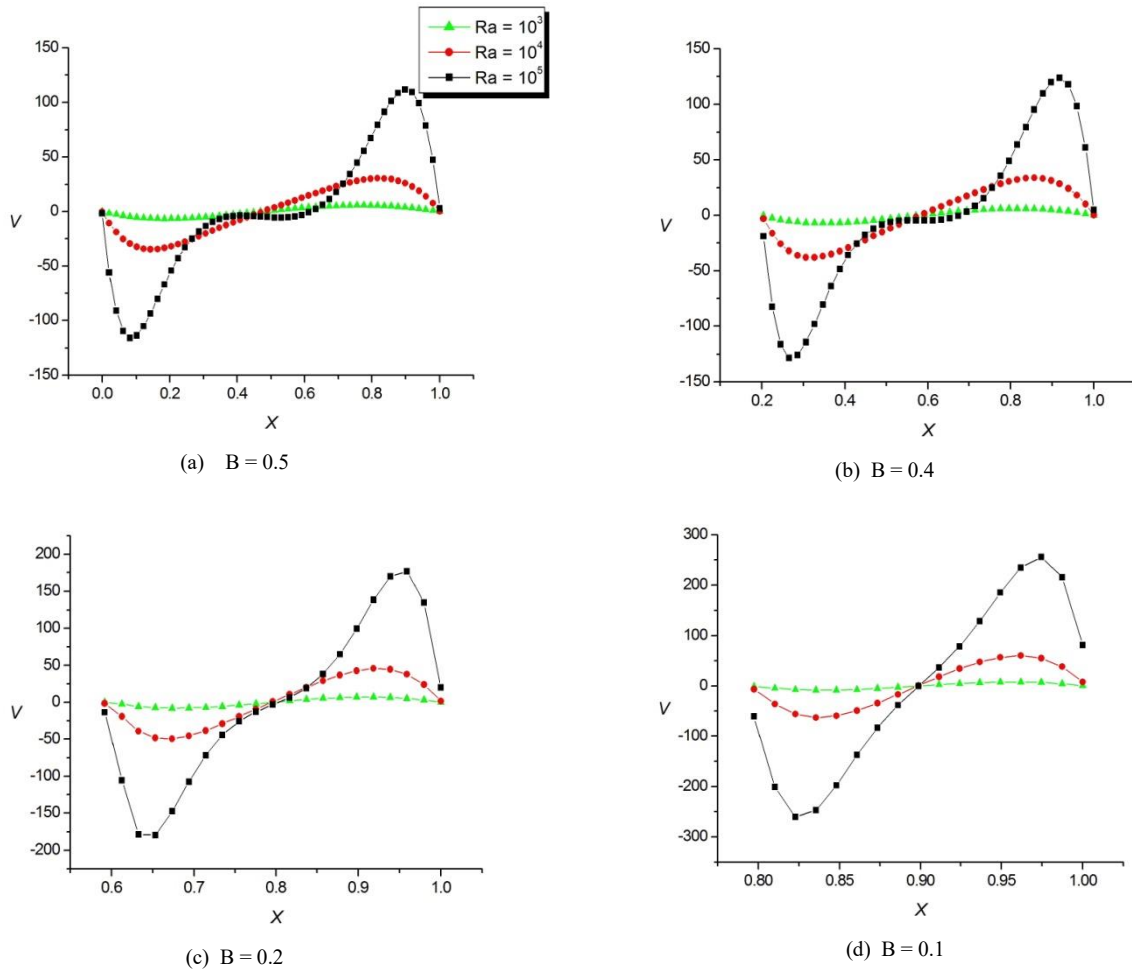


Figure 8. Dimensionless velocity profiles of V along X for various values of Ra and B at $Pr = 6.1$ related to (case 1).

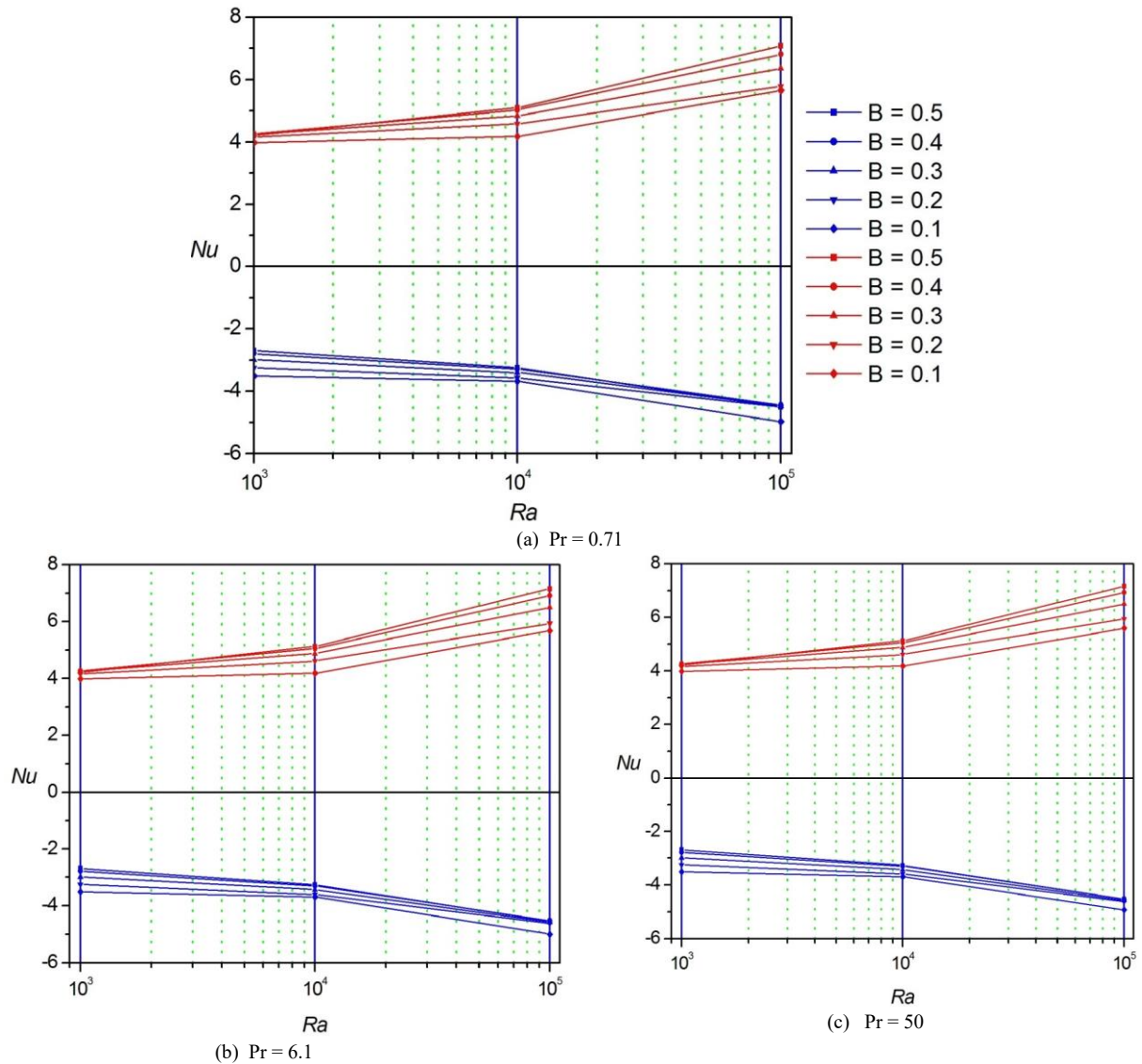


Figure 9. Profiles of mean Nu number versus Ra for different values of Pr and B related to (case 1).

4.2. Case 2 (Hot left arc and cold right arc):

In this case, the thermal distribution of the arcs was reversed. So, the left and right arcs were preserved at constant hot and cold temperatures, respectively. Figs. (10, 11 and 12) illustrate the streamlines and isotherms, respectively, inside the crescent shape cavity for various values of Ra , Pr and B related to (case 2). It can be observed from these figures that the pattern of the intra-compartment flow, in this case, is similar to that found in (case 1). However, a simple difference between them can be summarized in two points. The first point is that at $Ra = 10^5$, $B = 0.4$ and 0.5 , the core of vortices is affected by shifting the thermal boundary conditions of the arcs. Therefore, it can be concluded that they move towards the cold arc of the cavity for both considered cases. While this difference begins to disappear with the decrease in B values. Therefore, it could be deduced that the change of the thermal boundary conditions becomes discernible

when the buoyancy force has a substantial influence, and the cavity's width is big. The second point is that the minor vortices which are observed at $Ra = 10^5$ and $B = 0.1$ are replaced by their position from the bottom region in (Case 1) to the upper region in (Case 2). Once again, there is no discernible shift in the pattern of the streamlines when the (Pr) increases from $Pr = 0.71$ to 50 .

With respect to the isotherm contours, it was seen that the thermal plume was adjacent to the hot left arc and extended further inside the cavity until it attained the cold right arc. It can be observed by comparing the results in Fig.12 with that displayed in Fig.7 that the pattern of isotherms is similar to each other except adjacent to the arcs boundaries. In a similar manner discussed in (Case 1), the isotherm contours are highly influenced by increasing the Ra . Therefore, they switch their pattern from uniform lines for low Ra to a ripple-like pattern at high values. This behavior is due to the high-temperature gradient between the cavity's left hot and right cold arcs.

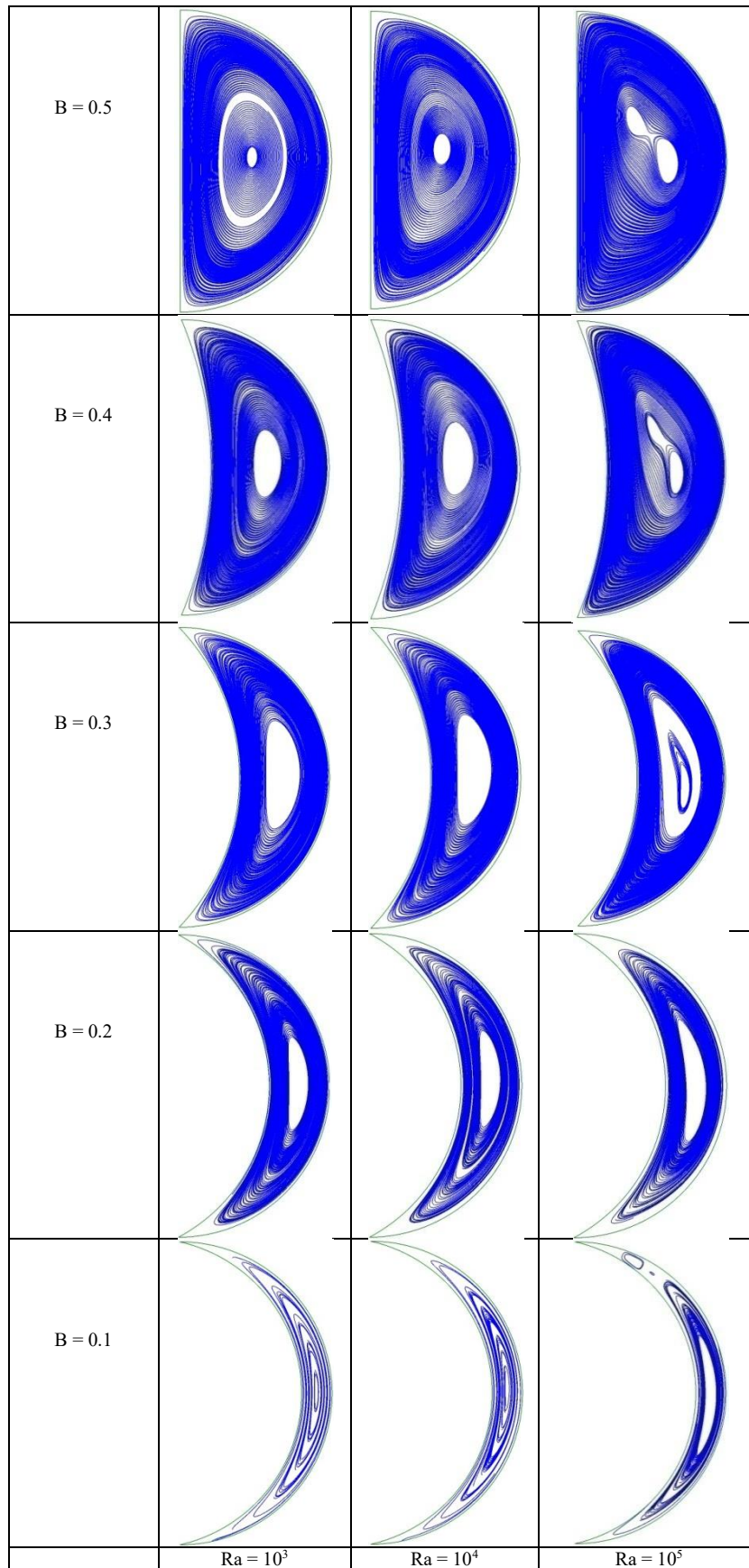


Figure 10. Streamlines inside the crescent shape cavity for various values of Ra and B at $Pr = 6.1$ related to (case 2).

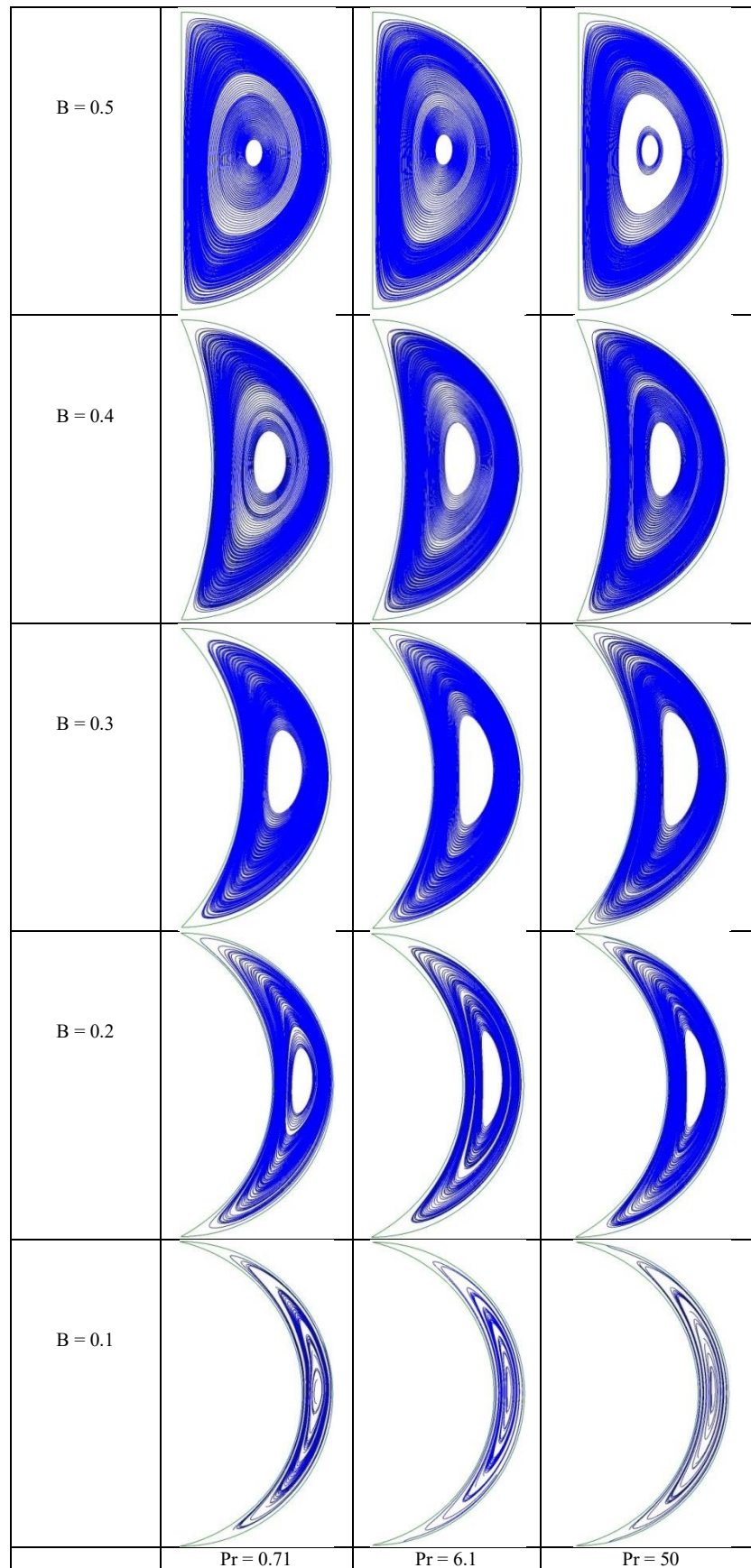


Figure 11. Streamlines inside the crescent shape cavity for various values of Pr and B at $Ra = 10^4$ related to (case 2).

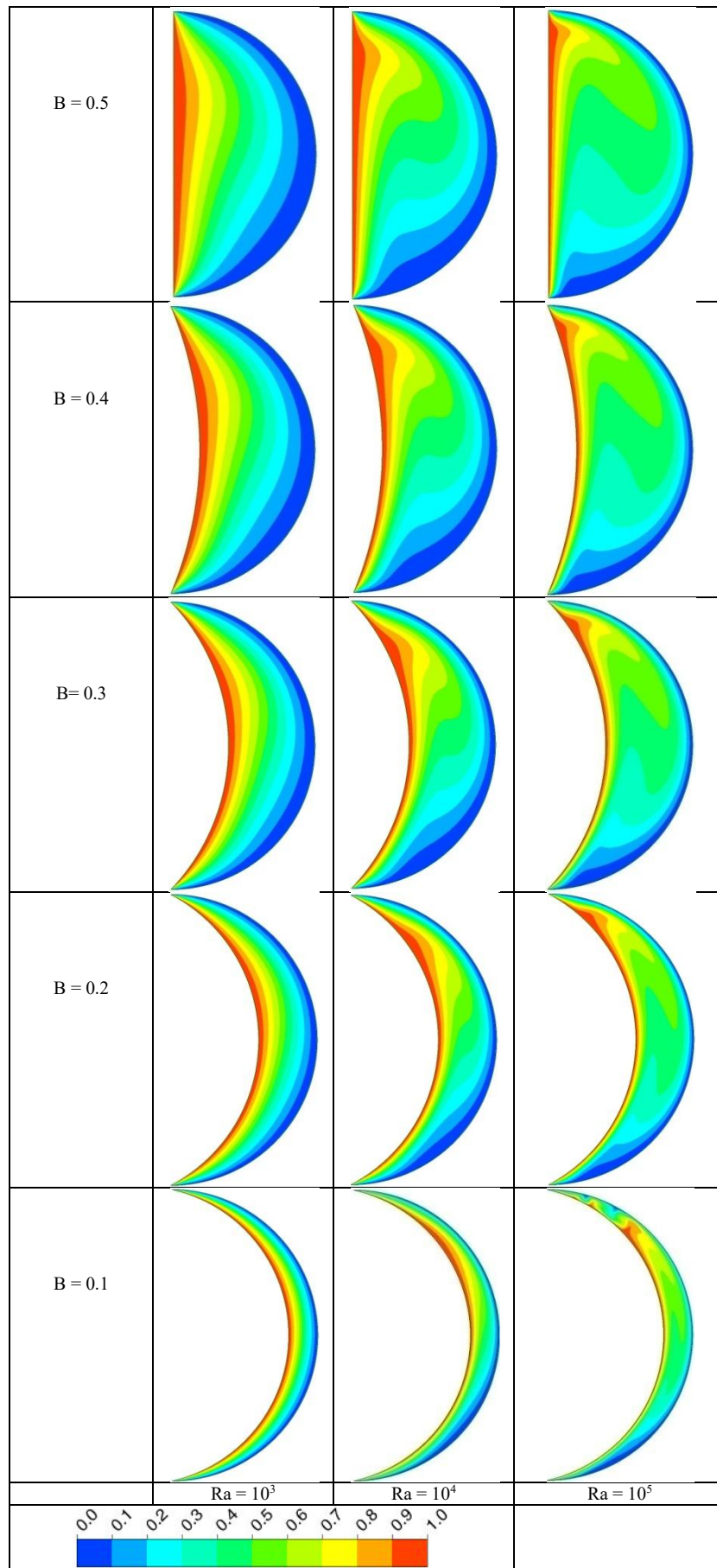


Figure 12. Isotherms inside the crescent shape cavity for various values of Ra and B at $Pr = 6.1$ related to (case 2).

The distribution of dimensionless velocity component V along with the width gap spacing for various values of Ra and B at $Pr = 6.1$ was displayed in Fig.13. The plus (+) and minus (-) signs indicate the direction of the movement of the fluid particles. This refers to the fact that adjacent to the cold right arc, the direction of the flow is downward, whereas, adjacent to the hot left arc, its direction is upward. Therefore, the velocity distribution was opposite to that noticed in Fig. 8. This result confirms that the velocity profiles are strongly affected by changing the thermal boundary conditions in cases 1 and 2. Similar to that found previously in (case 1), the velocity profiles increase with the increase in Ra and decrease in B . Therefore, their peak value can be found at $Ra = 10^5$ and $B = 0.1$.

The profiles of the mean values of Nu in terms of Ra , Pr and B were illustrated in Fig. 14. Again, the first set (the red lines) was related to the hot arc, whereas the second set (the blue lines) was related to the cold arc. Similar to that found previously in (case 1), the values of Nu are not varied clearly with the increase in Pr . This can be confirmed by the high similarity of Nu profiles for all selected values of Pr . The results indicated that Nu profiles for both cold and hot arcs increased with Ra . On another hand, the Nu was increased with the decrease in B for the hot arc, while an inverse effect can be seen for the cold arc. Furthermore, all observations and inferred analyzes agree with previous analyzes such as [68-75].

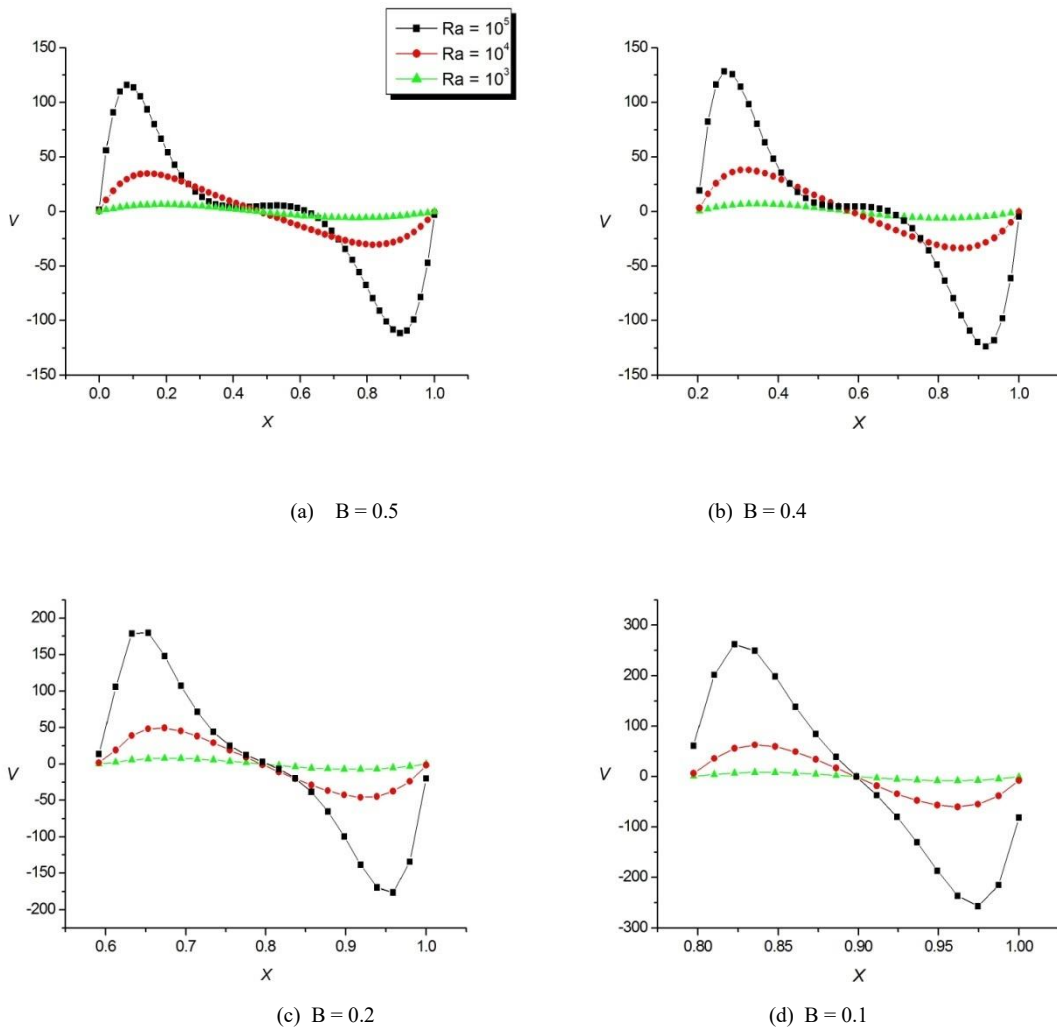


Figure13. Dimensionless velocity profiles of V along X for various values of Ra and B at $Pr = 6.1$ related to (case 2).

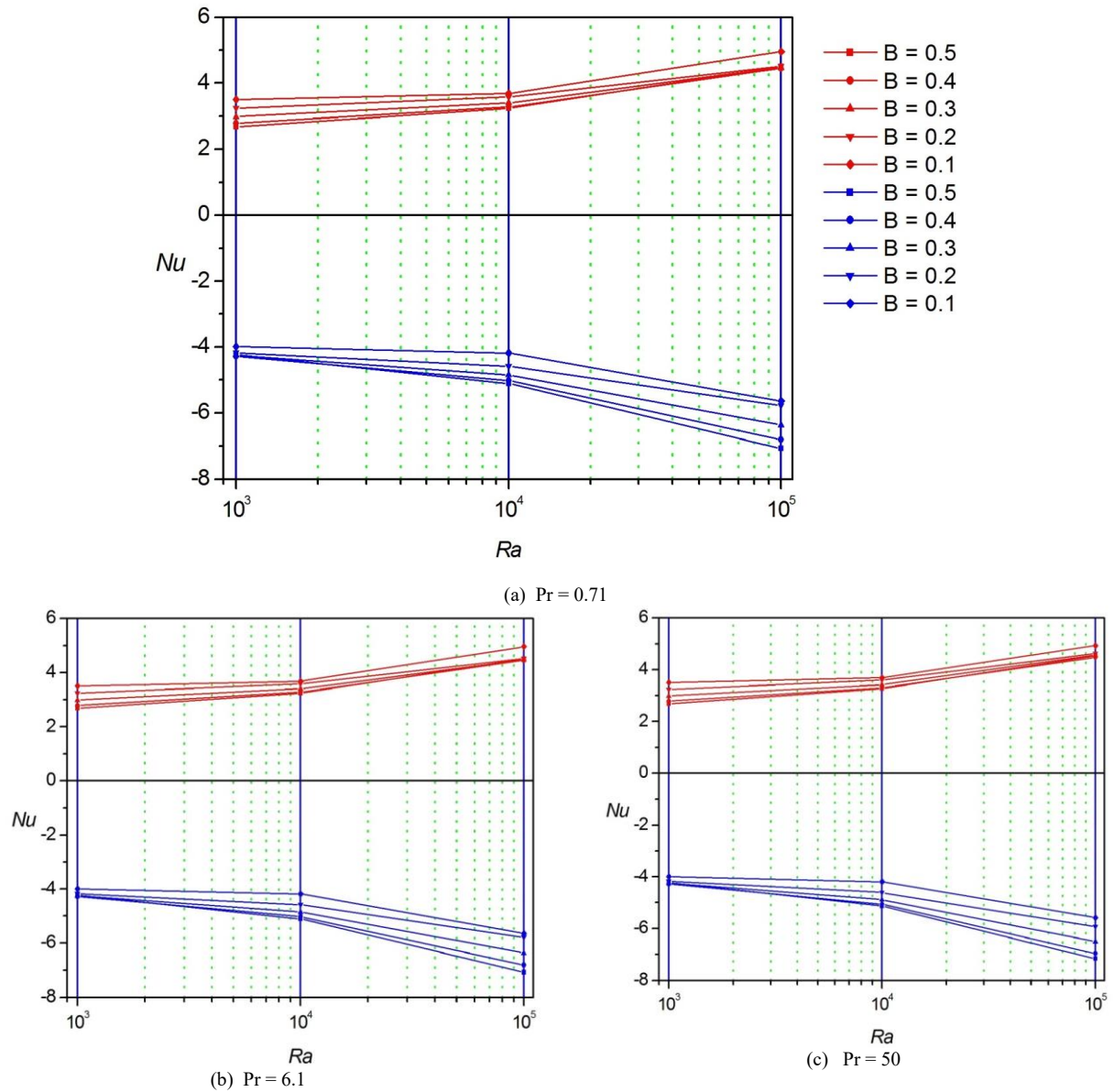


Figure 14. Profiles of mean Nu number versus Ra for different values of Pr and B related to (case 2).

5. Conclusions

The following are the key points that were extracted from the current work:

1. The flow velocity and buoyancy-driven convection increase as Ra increases in both considered cases.
2. For both considered cases, when the value of B decreases, the fluid movement becomes slow, and the flow pattern becomes approximately similar.
3. For both considered cases, the flow and thermal patterns were not affected by changing the fluid's thermal properties Pr .
4. For both considered cases, the velocity profiles increase with the increase in Ra and decrease in B . Therefore, their peak value can be found at $Ra = 10^5$ and $B = 0.1$. Also, the velocity profiles are affected strongly by changing the thermal boundary conditions.
5. For both considered cases, the increase in Ra increases the values of Nu for both arcs.
6. For (case 1), when the value of B decreases, the Nu for the hot arc decreases whereas its value for the cold arc begins to increase. For (case 2), the Nu was increased with the decrease in B for the hot arc, while an inverse effect can be seen for the cold arc.
7. When the influence of buoyancy force is substantial, and the cavity width is big, the shifting thermal boundary conditions become obvious.
8. These new kinds of results can be exploited in heat exchanger applications as well as insulating systems.
9. In future works, we suggest to use a fluid that combines rheological and nanoscale properties.

Acknowledgements

This publication was supported by the Deanship of Scientific Research at Prince Sattam bin Abdulaziz University, Alkharj, Saudi Arabia.

References

- [1] Gourari , S., Mebarek-Oudina, F., Hussein, A.K., Kolsi, L., Hassen, W. and Younis, O. Numerical study of natural convection between two coaxial inclined cylinders, International Journal of Heat and Technology, Vol. 37, No. 3, 2019, pp. 779-786.
- [2] Elkhazen, M., Hassen, W., Gannoun, R., Hussein, A.K. and Borjini, M. Numerical study of electro convection in a dielectric layer between two cofocal elliptical cylinders subjected to unipolar injection, Journal of Engineering Physics and Thermophysics, Vol. 92, No. 5, 2019, pp. 1318-1329.
- [3] Al-Rashed, A., Kolsi, L., Hussein, A. K., Hassen, W., Aichouni, M. and Borjini, M. Numerical study of three-dimensional natural convection and entropy generation in a cubical cavity with partially active vertical walls, Case Studies in Thermal Engineering, Vol. 10, 2017, pp: 100-110.
- [4] Ahmed, S., Hussein, A.K., Abd El-Aziz, M. and Sivasankaran, S. Conjugate natural convection in an inclined square porous enclosure with finite wall thickness and partially heated from its left sidewall. Heat Transfer Research, Vol.47, No.4, 2016, pp: 383-402.
- [5] Hussain, S. and Hussein, A.K. Numerical investigation of natural convection phenomena in a uniformly heated circular cylinder immersed in a square enclosure filled with air at different vertical locations, International Communications in Heat and Mass Transfer, Vol. 37, No.8, 2010, pp: 1115-1126.
- [6] Ghachem, K., Kolsi, L., Mâatki, C., Hussein, A.K. and Borjini, M. Numerical simulation of three-dimensional double diffusive free convection flow and irreversibility studies in a solar distiller, International Communications in Heat and Mass Transfer, Vol.39, 2012, pp: 869-876.
- [7] Kolsi , L. , Hussein, A.K. , Borjini, M. , Mohammed , H. and Ben Aïssia ,H. Computational analysis of three-dimensional unsteady natural convection and entropy generation in a cubical enclosure filled with water- Al_2O_3 nanofluid, Arabian Journal for Science and Engineering, Vol. 39, 2014, pp: 7483-7493.
- [8] Ahmed, S., Mansour, M., Hussein, A.K., Mallikarjuna, B., Al-Meshaal, M. and Kolsi, L. MHD mixed convection in an inclined cavity containing adiabatic obstacle and filled with Cu-water nanofluid in the presence of the heat generation and partial slip, Journal of Thermal Analysis and Calorimetry, Vol.138, No.2, 2019, pp: 1443-1460.
- [9] Nikbakhti, R., Wang, X., Hussein, A.K. and Iranmanesh, A. Absorption cooling systems - Review of various techniques for energy performance enhancement, Alexandria Engineering Journal, Vol. 59, 2020, pp: 707-738.
- [10] Sojoudi, A., Saha, S. and Gu, Y. Natural convection due to differential heating of inclined walls and heat source placed on bottom wall of an attic shaped space, Energy and Buildings, Vol. 89, 2015, pp: 153-162.
- [11] Hussein, A.K., Rout, S., Fathinia, F., Chand, R. and Mohammed, H. Natural convection in a triangular top wall enclosure with a solid strip, Journal of Engineering Science and Technology, Vol.10, No.10, 2015, pp: 1326 - 1341.
- [12] Hussein, A.K. and Hussain, S. Natural convection in a modified square enclosure with an inclined triangular top wall subjected to uniform heat flux in its left vertical wavy sidewall, Third Asian Symposium on Computational Heat Transfer and Fluid Flow, 22-26, September 2011, Kyoto, Japan, pp: 1-10.
- [13] Hussein, A.K. Entropy generation due to the transient mixed convection in a three-dimensional right-angle triangular cavity, International Journal of Mechanical Sciences, Vol.146-147, 2018, pp: 141-151.
- [14] Hussain, S., Hussein, A. and Mahdi, M. Natural convection in a square inclined enclosure with vee-corrugated sidewalls subjected to constant flux heating from below, Nonlinear Analysis: Modelling and Control, Vol. 16, No. 2, 2011, pp: 152-169.
- [15] Hussein, A.K., Hussain, S., Saha, S., Saha, G. and Hasanuzzaman, M. Effects of a longitudinal magnetic field and discrete isoflux heat source size on natural convection inside a tilted sinusoidal corrugated enclosure, Journal of Basic and Applied Scientific Research, Vol.3, No. 10, 2013, pp: 402-415.
- [16] Hussain, S., Hussein, A.K. and Mohammed, R. Studying the effects of a longitudinal magnetic field and discrete isoflux heat source size on natural convection inside a tilted sinusoidal corrugated enclosure, Computers and Mathematics with Applications, Vol. 64, 2012, pp: 476-488.
- [17] Hussein, A.K. and Hussain, S. Heatline visualization of natural convection heat transfer in an inclined wavy cavities filled with nanofluids and subjected to a discrete isoflux heating from its left sidewall, Alexandria Engineering Journal, Vol.55, 2016, pp: 169-186.
- [18] Mahfouz, F. Buoyancy driven flow within an inclined elliptic enclosure, International Journal of Thermal Sciences, Vol. 50 , 2011, pp : 1887-1899.
- [19] Hussain, S., Hussein, A. and Kadim, K. Numerical simulation of natural convection in a parallelogrammic enclosure containing volumetric heat source with non-uniformly heated left sidewall, Heat Transfer-Asian Research, Vol. 43, No.6, 2014, pp: 542-560.
- [20] Ghani, I., Khammas, F., Mustafa, A. and Hussein, A.K. MHD natural convection in a fully opened parallelogrammic enclosure filled with copper-water nanofluid and partially heated from its left sidewall, Journal of Advanced Research in Fluid Mechanics and Thermal Sciences, Vol. 74, No. 2, 2020, pp: 120 -145.
- [21] Hussein, A.K. and Mustafa, A. Natural convection in a fully open parallelogrammic cavity filled with Cu-water nanofluid and heated locally from its bottom wall, Thermal Science and Engineering Progress, Vol. 1, 2017, pp: 66-77.
- [22] Hussain, S. and Hussein, A.K. Natural convection heat transfer enhancement in a differentially heated parallelogrammic enclosure filled with copper-water nanofluid, Journal of Heat Transfer-Transactions of the ASME, Vol.136, 2014, pp: 082502-1- 082502-8.
- [23] Hussein, A.K. Finite volume simulation of natural convection in a trapezoidal cavity filled with various fluids and heated from the top wall, Universal Journal of Fluid Mechanics, Vol.1, 2013, pp: 24-36.
- [24] Hussein, A.K. and Mustafa, A. Natural convection in a parabolic enclosure with an internal vertical heat source filled with Cu-water nanofluid, Heat Transfer-Asian Research, Vol. 47, 2018, pp: 320-336.
- [25] Ziapour, B. and Dehnavi, R. Finite-volume method for solving the entropy generation due to air natural convection in C-shaped enclosure with circular corners, Mathematical and Computer Modelling, Vol. 54, 2011, pp: 1286-1299.
- [26] Hussein, A.K., Bakier , M., Ben Hamida , M. and Sivasankaran, S. Magneto-hydrodynamic natural convection in an inclined T-shaped enclosure for different nanofluids and subjected to a uniform heat source, Alexandria Engineering Journal, Vol. 55, 2016, pp: 2157-2169.
- [27] Sourtiji, E. and Hosseinizadeh, S. Heat transfer augmentation of magneto-hydrodynamics natural convection in L-shaped cavities utilizing nanofluids, Thermal Science, Vol.16, No.2, 2012, pp: 489-501.
- [28] Dehnavi, R. and Rezvani, A. Numerical investigation of natural convection heat transfer of nanofluids in a Γ shaped cavity, Superlattices and Microstructures, Vol. 52, 2012, pp: 312-325.

- [29] Fard, A., Hooshmand, P., Mohammaei, M. and Ross, D. Numerical study on free convection in a U-shaped CuO/water nanofluid-filled cavity with different aspect ratios using double-MRT lattice Boltzmann, *Thermal Science and Engineering Progress*, Vol. 14, 2019, 100373.
- [30] Yadollahi, A., Khalesidoost, A., Kasaeipoor, A., Hatami, M. and Jing, D. Physical investigation on silver-water nanofluid natural convection for an F-shaped cavity under the magnetic field effects, *The European Physical Journal Plus*, Vol. 132, 2017, pp: 372-384.
- [31] Dutta, S., Biswas, A. and Pati, S. Analysis of natural convection in a rhombic enclosure with undulations of the top wall - a numerical study, *International Journal of Ambient Energy*, 2019, <https://doi.org/10.1080/01430750.2019.1630304>.
- [32] Hussein, A.K. Computational analysis of natural convection in a parallelogrammic cavity with a hot concentric circular cylinder moving at different vertical locations, *International Communications in Heat and Mass Transfer*, Vol. 46, 2013, pp: 126-133.
- [33] Salih, E. and Mustafa, A. Natural convection in a parallelogrammic enclosure partially heated from below, *Zanco Journal of Pure and Applied Sciences*, Vol.26, No.3, 2014, pp: 43-60.
- [34] Anandalakshmi, R. and Basak, T. Heatline-based thermal management for natural convection in porous rhombic enclosures with isothermal hot side or bottom wall, *Energy Conversion and Management*, Vol. 67, 2013, pp: 287-296.
- [35] Adekeye, T., Adegun, I., Okekunle, P., Hussein, A. K., Oyedepo, S., Adetiba, E. and Fayomi, O. Numerical analysis of the effects of selected geometrical parameters and fluid properties on MHD natural convection flow in an inclined elliptic porous enclosure with localized heating, *Heat Transfer-Asian Research*, Vol. 46, No.3, 2017, pp: 261-293.
- [36] Hussain, S. and Hussein, A.K. Natural convection analysis around a hot solid circular cylinder embedded inside an octagonal enclosure at various orientation locations, *World Academy of Science, Engineering and Technology*, Vol. 78, 2013, pp: 1238-1243.
- [37] Chen, C. and Cheng, C. Buoyancy-induced flow and convective heat transfer in an inclined arc-shape enclosure, *International Journal of Heat and Fluid Flow*, Vol.23, 2002, pp: 823-830.
- [38] Tasnim, S. and Mahmud, S. Laminar free convection inside an inclined L-shaped enclosure, *International Communications in Heat and Mass Transfer*, Vol.33, 2006, pp: 936-942.
- [39] Mustafa, A. Natural convection in a parabolic enclosure heated from below, *Modern Applied Science*, Vol. 5, No. 3, 2011, pp: 213-220.
- [40] Wang, A., Ying, C., Wang, Y., Yang, L., Ying, Y., Zhai, L. and Zhang, W. Effect of orientation and aspect ratio of an internal flat plate on natural convection in a circular enclosure, *Processes*, Vol. 7, 2019, pp: 1-15.
- [41] Wang, Y., Chen, J. and Zhang, W. Natural convection in a circular enclosure with an internal cylinder of regular polygon geometry, *AIP Advances*, Vol. 9, 065023, 2019, doi: 10.1063/1.5100892.
- [42] Welhezi, H., Ben-Cheikh, N. and Ben-Beya, B. Numerical analysis of natural convection between a heated cube and its spherical enclosure, *International Journal of Thermal Sciences*, Vol. 150, 2020, Article No. 105828.
- [43] Roy, S., Tanmay, B., Thirumalesha, C. and Murali Krishna, C. Finite element simulation on natural convection flow in a triangular enclosure due to uniform and non-uniform bottom heating, *Journal of Heat Transfer*, Vol. 130, No.3, 2008, pp: 1761-1769.
- [44] Saha, S. Unsteady natural convection in a triangular enclosure under isothermal heating, *Energy and Buildings*, Vol. 43, 2011, pp: 695-703.
- [45] Oztop, H., Varol, Y., Koca, A. and Firat, M. Experimental and numerical analysis of buoyancy-induced flow in inclined triangular enclosures, *International Communications in Heat and Mass Transfer*, Vol. 39, 2012, pp: 1237-1244.
- [46] El-Hassan, R., Campo, A. and Chang, J. Natural convection patterns in right-angled triangular cavities with heated vertical sides and cooled hypotenuses, *Journal of Heat Transfer*, Vol. 127, No.10, 2005, pp: 1181-1186.
- [47] Yesiloz, G. and Aydin, O. Laminar natural convection in right-angled triangular enclosures heated and cooled on adjacent walls, *International Journal of Heat and Mass Transfer*, Vol. 60, 2013, pp: 365-374.
- [48] Mushatet, K. Simulation of natural convection in an inclined square cavity with two wavy walls, *Journal of Applied Sciences Research*, Vol.6, No.12, 2010, pp: 2111-2122.
- [49] Adjlout, L., Imine, O., Azzi, A. and Belkadi, M. Laminar natural convection in an inclined cavity with a wavy wall, *International Journal of Heat and Mass Transfer*, Vol. 45, 2002, pp: 2141-2152.
- [50] Koulali, A., Sahi, A., Meziani, B., Aissa, A., Sadaoui, D. and Ali, H. CFD analysis of natural convection between two superposed fluids: role of corrugated bottoms, *Chemical Engineering Communications*, 2021, <https://doi.org/10.1080/00986445.2021.1976162>
- [51] Hussein, A.K., Kolsi, L., Chand, R., Sivasankaran, S., Nikbakhti, R., Li, D., Borjini, M. and Ben Aïssia, H. Three-dimensional unsteady natural convection and entropy generation in an inclined cubical trapezoidal cavity with an isothermal bottom wall, *Alexandria Engineering Journal*, Vol.55, 2016, pp: 741-755.
- [52] Natarajan, E., Basak, T. and Roy, S. Natural convection flows in a trapezoidal enclosure with uniform and non-uniform heating of bottom wall, *International Journal of Heat and Mass Transfer*, Vol.51, 2008, pp: 747-756.
- [53] Lasfer, K., Bouzaiane, M. and Lili, T. Numerical study of laminar natural convection in a side-heated trapezoidal cavity at various inclined heated sidewalls, *Heat Transfer Engineering*, Vol. 31, No.5, 2010, pp: 362-373.
- [54] Dutta, S., Goswami, N., Pati, S. and Biswas, A. Natural convection heat transfer and entropy generation in a porous rhombic enclosure: influence of non-uniform heating, *Journal of Thermal Analysis and Calorimetry*, Vol. 144, 2021, pp: 1493-1515.
- [55] Garcia de Maria, J., Baïri, A. and Costa, V. Empirical correlations at high Ra for steady-state free convection in 2D air-filled parallelogrammic enclosures with isothermal discrete heat sources, *International Journal of Heat and Mass Transfer*, Vol. 53, 2010, pp: 3831-3838.
- [56] Hussain, S., Hussein, A. and Kadim, K. Numerical simulation of natural convection in a parallelogrammic enclosure containing volumetric heat source with non-uniformly heated left sidewall, *Heat Transfer-Asian Research*, Vol. 43, No.6, 2014, pp: 542-560.
- [57] Mahmud, S., Das, P., Hyder, N. and Islam, A. Free convection in an enclosure with vertical wavy walls, *International Journal of Thermal Sciences*, Vol. 41, 2002, pp: 440-446.
- [58] Alnaqi, A., Hussein, A. K., Kolsi, L., Al-Rashed, A., Li, D. and Ali, H. Computational study of natural convection and entropy generation in the 3-D cavity with active lateral walls, *Thermal Science*, Vol. 24, No. 3B, 2020, pp: 2089-2100.
- [59] Li, Z., Hussein, A.K., Younis, O., Rostami, S. and He, W. Effect of alumina nano-powder on the natural convection of water under the influence of a magnetic field in a cavity and optimization using RMS: Using empirical correlations for the thermal conductivity and sensitivity analysis, *International*

- Communications in Heat and Mass Transfer, Vol. 112, Article No. 104497, 2020.
- [60] Bendejina, A., Imine, O. and Adjlout, L. Laminar free convection in undulated cavity with non-uniform boundary conditions, *Comptes Rendus Mecanique*, Vol.339, 2011, pp: 42-57.
- [61] Ghachem, K., Hussein, A.K., Kolsi, L. and Younis, O. CNT-water nanofluid magneto-convective heat transfer in a cubical cavity equipped with perforated partition, *The European Physical Journal Plus*, Vol. 136: 377, 2021, pp: 1-22.
- [62] Zhang, X. and Hussein, A.K. Asymptotic solution of natural convection in a uniformly Joule-heating shallow cavity, *Journal of Physics: Conference Series*, Vol. 574 (012156), 2015, pp: 1-4.
- [63] Li, Z., Hussein, A.K., Younis, O., Afrand, M. and Feng, S. Natural convection and entropy generation of a nanofluid around a circular baffle inside an inclined square cavity under thermal radiation and magnetic field effects, *International Communications in Heat and Mass Transfer*, Vol. 116, Article No. 104650, 2020.
- [64] Hussein, A.K., Ashorynejad, H., Sivasankaran, S., Kolsi, L., Shikholeslami, M. and Adegun, I. Modeling of MHD natural convection in a square enclosure having an adiabatic square-shaped body using Lattice Boltzmann Method, *Alexandria Engineering Journal*, Vol.55, 2016, pp: 203-214.
- [65] Barakos, G., Mitsoulis, E. and Assimacopoulos, D. Natural convection flow in a square cavity revisited: laminar and turbulent models with wall functions, *International Journal for Numerical Methods in Fluids*, Vol. 18, 1994, pp: 695-719.
- [66] Kuehn, T. and Goldstein, R. An experimental study of natural convection heat transfer in concentric and eccentric horizontal cylindrical annuli, *ASME Journal of Heat Transfer*, Vol. 100, No.4, 1978, pp: 635-640.
- [67] Matin, M. and Khan, A. Laminar natural convection of non-Newtonian power-law fluids between concentric circular cylinders, *International Communications in Heat and Mass Transfer*, Vol. 43, 2013, pp: 112-121.
- [68] Kumar, M. and Mondal, P.K. Bejan's flow visualization of buoyancy-driven flow of a hydromagnetic Casson fluid from an isothermal wavy surface, *Physics of Fluids*, Vol., 33, 2021, pp: 093113.
- [69] Kumar, M. and Mondal, P.K. Buoyancy driven flow of a couple stress fluid from an isothermal vertical plate: the role of spatially periodic magnetic field, *Physica Scripta*, Vol., 96, 2021, pp: 125014.
- [70] DasGupta D., Mondal P.K., Chakraborty S. Thermocapillary-actuated contact-line motion of immiscible binary fluids over substrates with patterned wettability in narrow confinement, *Physical Review E*, 90, 2014, pp: 023011.
- [71] Mondal P.K., Chaudhry S. Effects of gravity on the thermo-hydrodynamics of moving contact lines, Vol.30, 2018, pp: 042109.
- [72] Rashid F.L., Talib S. M., Hussein A. K., ObaiY., An Experimental Investigation of Double Pipe Heat Exchanger Performance and Exergy Analysis Using Air Bubble Injection Technique, *Jordan Journal of Mechanical and Industrial Engineering*, Vol.16, 2022, pp:195-204.
- [73] Yadav A. S., Effect of Half Length Twisted-Tape Turbulators on Heat Transfer and Pressure Drop Characteristics inside a Double Pipe U-Bend Heat Exchanger, *Jordan Journal of Mechanical and Industrial Engineering*, Vol. 3, 2009, pp: 17-22.
- [74] Hossain R.A., Chowdhuri M.A.K, Feroz C. M., Design, Fabrication and Experimental Study of Heat Transfer Characteristics of a Micro Heat Pipe, *Jordan Journal of Mechanical and Industrial Engineering*, Vol. 4, 2010, pp:531-542.
- [75] Murali G. J. , Katte S. S., Experimental Investigation of Heat Transfer Enhancement in Radiating Pin Fin, *Jordan Journal of Mechanical and Industrial Engineering*, Vol. 2, 2008, pp:163-167.